International Journal of Nanomedicine

Dovepress
open access to scientific and medical research

Open Access Full Text Article

ORIGINAL RESEARCH

Rescuing cholinergic neurons from apoptotic degeneration by targeting of serotonin modulator- and apolipoprotein E-conjugated liposomes to the hippocampus

This article was published in the following Dove Press journal:
International Journal of Nanomedicine
15 December 2016
Number of times this article has been viewed

Yung-Chih Kuo
Yin-Jung Lee

Department of Chemical Engineering, National Chung Cheng University, Chia-Yi, Taiwan, Republic of China

Abstract: β-Amyloid (Aβ)-targeting liposomes (LIP) with surface serotonin modulator (SM) and apolipoprotein E (ApoE) were utilized to facilitate the delivery of nerve growth factor (NGF) across the blood–brain barrier (BBB) for neuroprotection in the hippocampus. The therapeutic efficacy of SM- and ApoE-grafted LIP carrying NGF (NGF-SM-ApoE-LIP) was assessed by an in vitro Alzheimer's disease (AD) model of degenerated SK-N-MC cells and an in vivo AD model of Aβ-insulted Wistar rats. The experimental evidences revealed that the modified SM and ApoE on the surface of LIP increased the permeation of NGF across the BBB without serious damage to structural integrity of tight junction. When compared with free NGF, NGF-SM-ApoE-LIP upregulated the expression of phosphorylated neurotrophic tyrosine kinase receptor type 1 on cholinergic neurons and significantly improved their survival. In addition, NGF-SM-ApoE-LIP could reduce the secretion of acetylcholinesterase and malondialdehyde and rescue hippocampal neurons from apoptosis in rat brains. The synergistic effect of SM and ApoE is promising in the induction of NGF to inhibit the neurotoxicity of Aβ and NGF-SM-ApoE-LIP can be a potent antiapoptotic pharmacotherapy for clinical care of patients with AD.

Keywords: Alzheimer's disease, blood–brain barrier, serotonin modulator, apolipoprotein E, nerve growth factor, liposome

Introduction

Alzheimer's disease (AD) is a formidable chronic neurodegenerative disorder resulting primarily from the abnormal deposition of β-amyloid (Aβ) around neurons and the formation of senile plaques and neurofibrillary tangles by hyperphosphorylation of tau protein in the hippocampus.[1] In addition to the dementia of episodic mental disability and poor health, the evolution of AD leads eventually to the death of patients (on average living for 9 years after diagnosis).[2] Nerve growth factor (NGF), a cardinal neurotrophic factor in neural circuits, can be a competent remedy for AD management. In fact, NGF can stimulate distal neurites and upregulate neurotrophic tyrosine kinase receptor type 1 (TrkA) for neuronal survival, growth, and differentiation in nervous system.[3] TrkA evokes subsequent intracellular signaling cascades, including Ras/Raf/mitogen-activated protein kinase, phosphoinositide phospholipase C-γ, and phosphatidylinositol-4,5-bisphosphate 3-kinase/protein kinase B, to improve neuroprotective and neural repair functions.[4] In an organotypic brain slice model, the application of NGF protected cholinergic basal nuclei of Meynert neurons against

Correspondence: Yung-Chih Kuo
Department of Chemical Engineering, National Chung Cheng University, Chia-Yi, Taiwan 62102, Republic of China
Tel +886 5 272 0411 ext 33459
Fax +886 5 272 1206
Email chmyck@ccu.edu.tw

submit your manuscript | www.dovepress.com
Dovepress
http://dx.doi.org/10.2147/IJN.S123442

neurodegeneration, provided an insightful solution to neural rescue.[5] As a result, NGF increased neuronal survival. However, the problem of low permeability of NGF across the blood–brain barrier (BBB) has restrained its clinical efficacy from treating brain-related diseases. For example, an administration of NGF in cerebral ventricle could slightly ameliorate the neuropsychological index with an unclear cognitive improvement in a preclinical trial.[6] Therefore, instead of direct infusion, the utilization of targeting molecules to regulate the delivery of NGF can be a practical approach to control the progression of AD.

Serotonin was first employed as an antimigraine agent that inhibits synthesis of intracranial neurosensory peptides such as serotonin modulator (SM).[7] A release of the neuropeptide might activate second-order sensory neurons. In addition to the interaction with serotonin, SM has been found to specifically interact with serotonin receptor (SR) on endothelia of brain microvessels.[8,9] Hence, it is possible that an incorporation of SM in medicinal preparation may modify the neural activity in the brain for AD therapy. Moreover, apolipoprotein E (ApoE) could aid in crossing the BBB via low-density lipoprotein receptor (LDLR) and help avoid the decomposition of pharmaceuticals by lysosomes.[10,11] In lipid transport pathways, ApoE-containing lipoproteins could be cholesterol carriers and participate in metabolism and clearance related to pathophysiology of neurological diseases in the central nervous system (CNS).[12,13] It has also been observed that LDLR could mediate the ApoE variation induced by Aβ and translate the extracellular Aβ signal into cellular responses.[14] Therefore, a conjugation of ApoE in the drug delivery system can be potentially used for AD treatment.

The aim of this study was to develop SM- and ApoE-grafted liposomes (LIP) carrying NGF (NGF-SM-ApoE-LIP) and to evaluate the efficiency of NGF-SM-ApoE-LIP in neural salvage. In addition to SM and ApoE, cardiolipin (CL) was incorporated in LIP to dock Aβ because CL has a strong affinity to Aβ. Since Aβ plaque emerges in degenerated AD brains, targeting Aβ would improve the delivery of NGF to apoptotic neurons and slow AD progression. Thus, the combination of NGF, SM, ApoE, and CL can have profound influences on disease modification and receptor targeting for AD pharmacotherapy. In this study, the influence of NGF-SM-ApoE-LIP on endothelia and neurons are highlighted, including the BBB permeability, expression of phosphorylated TrkA (p-TrkA), secretion of acetylcholinesterase (AChE) and malondialdehyde (MDA), and distribution of neurons in the hippocampus.

Materials and methods

Preparation of NGF-SM-ApoE-LIP

Synthesis of NGF-LIP

1,2-Dipalmitoyl-*sn*-glycero-3-phosphocholine (DPPC; Avanti Polar Lipids, Alabaster, AL, USA), soybean phosphatidylcholine (SPC; Sigma-Aldrich, St Louis, MO, USA), cholesterol (Sigma-Aldrich), 1′,3′-bis[1,2-dimyristoyl-*sn*-glycero-3-phospho]-*sn*-glycerol (CL; Avanti Polar Lipids), palmitic acid (Sigma-Aldrich), and 1,2-distearoyl-*sn*-glycero-3-phosphoethanolamine-*N*-[carboxy(polyethylene glycol)-2000] (DSPE-PEG(2000)-CA; Avanti Polar Lipids) were mixed in 1 mL of chloroform (JT Baker, Phillipsburg, NJ, USA) at 25°C. In the case without CL, the molar percentage of DPPC, SPC, cholesterol, palmitic acid, and DSPE-PEG(2000)-CA in lipids was controlled at 40%, 10%, 40%, 7%, and 3%, respectively. When CL was included, the molar percentage of lipids was the same as above, except for DPPC. In this case, the molar percentage of DPPC and CL was 40% of total lipid. The lipid bilayer of LIP was formulated with these ingredients. Fluorescent liposomes were prepared by addition of 0.1% (w/v) fluorescein isothiocyanate-conjugated dextran 70,000 (Sigma-Aldrich) in the lipid phase. The lipids were deposited in a 50 mL round bottom flask by volatilization of chloroform using a rotary evaporator (Panchum, Kaohsiung, Taiwan) and a vacuum pump at 75 rpm and 45°C for 15 min. To prepare LIP-carrying NGF (NGF-LIP), the deposited thin solid membrane was hydrated with Dulbecco's phosphate-buffered saline (DPBS; Sigma-Aldrich) containing human β-NGF (Alomone Labs, Jerusalem, Israel) of 50 ng/mL at lipid concentration of 2 mg/mL and 45°C, vibrated at 46 kHz and 45°C for 30 min, and squeezed through a polycarbonate membrane (100 nm pore, Avanti Polar Lipids) 15 times using an extruder set (Avanti Polar Lipids). The suspension of NGF-LIP was separated using a packed column of swollen Sephadex G-100 powders (GE Healthcare, Piscataway, NJ, USA) at 25°C. Effluents from the upright glass column were collected to quantify NGF encapsulated in liposomes and determined with human NGF kit (Abcam, Cambridge, MA, USA) using an enzyme-linked immunosorbent assay (ELISA) spectrophotometer (Bio-tek, Winooski, VT, USA) at 450 nm. The entrapment efficiency of NGF in liposomes was calculated by using the formula [(weight of encapsulated NGF)/(weight of total NGF)] ×100%.

Grafting of SM and ApoE on NGF-LIP

The suspension of NGF-LIP in 2-(N-morpholino)ethanesulfonic acid (Sigma-Aldrich) was activated with 1 mM 1-ethyl-3-(3-dimethylaminopropyl)carbodiimide

(Sigma-Aldrich) and 1.5 mM *N*-hydroxysuccinimide (Alfa Aesar, Ward Hill, MA, USA) at 80 rpm and 25°C for 1.5 h, mixed with $ApoE_{131–169}$ (AnaSpec, Fremont, CA, USA) at 80 rpm and 25°C for 12 h, and isolated with the Sephadex G-100 column at 25°C. The quantity of free $ApoE_{131–169}$ was evaluated with a QuantiPro bicinchoninic acid (BCA) kit (Sigma-Aldrich) for protein concentrations in the range of 0.5–30 μg/mL and determined using the ELISA spectrophotometer at 562 nm. The grafting efficiency of $ApoE_{131–169}$ on NGF-LIP, G_{ApoE}, was defined as G_{ApoE} (%) and given by the formula [(weight of total $ApoE_{131–169}$ − weight of unloaded $ApoE_{131–169}$)/(weight of total $ApoE_{131–169}$)] ×100%. In addition, the suspension of NGF-LIP was mixed with SM (Leu-Ser-Ala-Leu; Kelowna International Scientific, Taipei, Taiwan) at 80 rpm and 4°C for 6 h, isolated with the Sephadex G-100 column at 25°C, and assayed with the BCA kit using the ELISA spectrophotometer at 562 nm. The grafting efficiency of SM on ApoE-grafted NGF-LIP (NGF-ApoE-LIP), G_{SM}, was defined as G_{SM} (%) and given by the formula [(weight of total SM − weight of unloaded SM)/(weight of total SM)] ×100%.

Characterization of NGF-SM-ApoE-LIP

Average diameter and zeta potential of NGF-SM-ApoE-LIP

The cumulant Z-average diameter, *D* (nm), and zeta potential, ζ (mV), of SM-grafted NGF-ApoE-LIP (NGF-SM-ApoE-LIP) were evaluated using a zetasizer 3000 HS_A with a photon correlation spectroscope and a laser Doppler velocimeter (Malvern, Worcestershire, UK) at 25°C. A suspension of NGF-SM-ApoE-LIP of 2 mg/mL in tris hydroxymethyl aminomethane (tris; Riedel-de Haen, Seelze, Germany) buffer at pH 7.4 was used in this study.

Morphology of NGF-SM-ApoE-LIP

The surface structure of NGF-SM-ApoE-LIP was examined using a field emission scanning electron microscope (FE-SEM; JSM-6330 TF, Jeol, Tokyo, Japan). The suspension of NGF-SM-ApoE-LIP of 2 mg/mL in tris buffer was vibrated ultrasonically for 1 min, loaded on a cover slip, dehumidified in air at 25°C for 24 h, vacuum dried, glued with carbon paint, and sputter-coated with platinum at accelerating voltage of 3 kV for 90 s. In addition, the geometry of NGF-SM-ApoE-LIP was investigated using a transmission electron microscope (TEM; JEM-1400, Jeol, Tokyo, Japan). The suspension of NGF-SM-ApoE-LIP of 2 mg/mL in tris buffer was dripped down on a 200-mesh copper grid with carbon coating for 1 min and counterstained with 2% (w/v) phosphotungstic acid (Sigma-Aldrich) solution for 2 min.

XPS spectra of NGF-SM-ApoE-LIP

The surface atoms on NGF-SM-ApoE-LIP were examined using an X-ray photoelectron spectroscope (XPS, Kratos, Kanagawa, Japan) in a light beam area of 300×700 mm at vacuum grade of $2×10^7$ Pa and at 300 W. The suspension of NGF-SM-ApoE-LIP of 2 mg/mL was dropped uniformly onto a cover slide of 5×5 mm, dehumidified, and vacuum dried for 15 min.

Influence of NGF-SM-ApoE-LIP on HBMEC/HA

Viability of HBMECs and HAs after treating with NGF-SM-ApoE-LIP

The culture methods for human brain-microvascular endothelial cells (HBMECs; Biocompare, South San Francisco, CA, USA) and human astrocytes (HAs; Sciencell, Carlsbad, CA, USA) have been published previously.[15] HBMECs or HAs were added to a gelatin-coated 96-well microwell plate and cultured at a density of $7.5×10^3$ cells/well with 150 μL of endothelial cell medium (Sciencell) or astrocyte medium (Sciencell) per well. The cells were incubated in an incubator (NuAire, Plymouth, MN, USA) with 95% relative humidity and 5% CO_2 at 37°C for 8 h. NGF-SM-ApoE-LIP was sterilized in a biological safety cabin with ultraviolet (UV) for 10 min before experiments. Seeded HBMECs and HAs were allowed to interact with 0.025% (w/v) NGF-SM-ApoE-LIP in the humidified CO_2 incubator for 16 h. The viability of HBMECs and HAs was assayed with 2,3-bis-(2-methoxy-4-nitro-5-sulfophenyl)-2H-tetrazolium-5-carboxanilide (XTT; Biological Industries, Beit Haemek, Israel) and evaluated using the ELISA spectrophotometer at 450 nm. HBMECs or HAs were reacted with 50 μL of the XTT solution containing 2% (v/v) activation component per well in the humidified CO_2 incubator for 4 h. The viability of HBMECs and HAs was defined as P_{CV} (%) = [(optical density of HBMECs or HAs treated with NGF-SM-ApoE-LIP − optical density of XTT)/(the optical density of HBMECs or HAs − optical density of XTT)] ×100%.

Transport of NGF-SM-ApoE-LIP across HBMEC/HA

The method for establishing a BBB model comprising a monolayer of HBMECs regulated by HAs (HBMEC/HA) on a gelatin-coated porous polyethylene terephthalate membrane (BD Falcon, Franklin Lakes, NJ, USA) in a transwell has been described previously.[16] To the upper chamber mimicking the blood side, 0.025% (w/v) NGF-SM-ApoE-LIP was added; it was then incubated in the humidified CO_2 incubator for 4 h. The electrical resistance of supporting membrane

with HBMEC/HA was evaluated using a Millicell electrical resistance system (Millipore, Billerica, MA, USA). The transendothelial electrical resistance (TEER) of HBMEC/HA was calculated by TEER ($\Omega\times$ cm^2) = (electrical resistance of supporting membrane with HBMEC/HA − electrical resistance of cell-free supporting membrane) × surface area of supporting membrane. After treating with 0.025% (w/v) NGF-SM-ApoE-LIP, 0.25 mg/mL propidium iodide (PI) was added to the medium in the upper chamber and incubated for 5 h. The quantity of PI in the lower chamber, mimicking the brain side, was evaluated using the ELISA spectrophotometer at excitation wavelength of 485 nm and emission wavelength of 590 nm. The permeability coefficient of PI across HBMEC/HA (P_{PI}) was calculated using the formula P_{PI} (cm/s) = [(permeability coefficient of PI across supporting membrane with HBMEC/HA)$^{-1}$ − (permeability coefficient of PI across supporting membrane)$^{-1}$]$^{-1}$. In addition, for transporting NGF across HBMEC/HA on supporting membrane, 0.025% (w/v) NGF-SM-ApoE-LIP was added to the upper chamber followed by incubation in the humidified CO_2 incubator for 5 h. The fluid in the lower chamber (20 µL) was treated with 1% (v/v) Triton-X-100 (Acros, Morris, NJ, USA) at 4°C for 1 h and assayed with human NGF kit using the ELISA spectrophotometer at 450 nm every 2.5 h. The volume of fluid in the lower chamber was balanced with an equal amount of fresh medium. The permeability coefficient of NGF across HBMEC/HA (P_{NGF}) can be obtained analogously to that of P_{PI} defined earlier.

Immunochemical staining of NGF-SM-ApoE-LIP and HBMECs

HBMECs were seeded on a gelatin-coated microscope cover glass at a density of 1×10^5 cells/cm^2 in a 24-well culture plate, cultured in the humidified CO_2 incubator for 8 h, and allowed to react with 0.025% (w/v) fluorescent NGF-SM-ApoE-LIP in the humidified CO_2 incubator for 3 h. The sample was immersed in 10% (v/v) formalin (Sigma-Aldrich) at 25°C for 10 min, permeated with 0.5% (v/v) Triton-X-100 at 25°C for 10 min, treated with serum blocking solution (Zymed, South San Francisco, CA, USA) at 25°C for 30 min, reacted with rabbit monoclonal antibody to human LDLR (Abcam) in a dilution ratio of 1:100 at 4°C for 12 h and/or guinea pig antibody to human SR (Chemicon, Temecula, CA, USA) in a dilution ratio of 1:300 at 25°C for 8 h, incubated with goat polyclonal antibody to mouse immunoglobulin G (IgG) (heavy and light [H+L]) (Abcam) in a dilution ratio of 1:100 at 25°C for 1 h, stained with 0.5% (w/v) 4′,6-diamidino-2-phenylindole (DAPI; Sigma-Aldrich) in 0.1% (v/v) Triton-X-100 at 25°C for 3 min, and maintained in aqueous mounting medium (Bio SB, Santa Barbara, CA, USA). Fluorescent images were obtained using a confocal laser scanning microscope (LSM 510, Zeiss, Oberkochen, Germany) with excitation wavelengths 350 nm (blue), 490 nm (green), and 555 nm (red) and emission wavelengths 475 nm (blue), 520 nm (green), and 565 nm (red).

Influence of NGF-SM-ApoE-LIP on degenerated SK-N-MC cells

Viability of A$\beta_{1\text{-}42}$-insulted SK-N-MC cells after treating with NGF-SM-ApoE-LIP

The methods for producing fibrillar A$\beta_{1\text{-}42}$ (Life Technologies, Carlsbad, CA, USA) by acidification and for expanding neuron-like SK-N-MC cells (American Type Tissue Collection, Rockville, MD, USA) have been described previously.[17] The study on the viability of SK-N-MC cells was similar to that of HBMECs and HAs except for the addition of NGF-SM-ApoE-LIP associated with 10 µM fibrillar A$\beta_{1\text{-}42}$. The viability of SK-N-MC cells, $P_{CV,\ SK\text{-}N\text{-}MC}$, was defined analogously as that of HBMECs and HAs (P_{CV}).

Western blot of p-TrkA after treating with NGF-SM-ApoE-LIP

SK-N-MC cells were incubated in a 12-well tissue culture microtiter plate at a density of 1×10^5 cells/well, treated with NGF-SM-ApoE-LIP at concentration of 4.7 ng NGF/well associated with 10 µM fibrillar A$\beta_{1\text{-}42}$, and decomposed with 200 µL of lysis buffer (Abcam) per well for 30 min. 2 µL of the lysed protein solution was diluted with 198 µL of ultrapure water (Barnstead, Dubuque, IA). 150 µL of the diluted sample was assayed with 150 µL of Coomassie blue protein assay kit (Thermo Fisher Scientific, St Waltham, MA, USA) in a 96-well plate and evaluated using the ELISA spectrophotometer at 595 nm. After thermal treatment at 95°C, the sample was added to 25% (v/v) sample buffer (Millipore) with 25 µg of the total protein per vial for sodium dodecyl sulfate–polyacrylamide gel (Sigma-Aldrich) electrophoresis. The proteins migrated in the separating gel at 60 V for 15 min and at 120 V for 30 min, were transferred to polyvinylidene fluoride (GE Healthcare, Buckinghamshire, UK) membranes in transfer buffer (Bio-Rad, Hercules, CA, USA) at 400 mA and 4°C for 90 min, blocked with 5% (w/v) skim milk for 1 h, reacted with anti-p-TrkA (Millipore) and anti-GAPDH (Cell Signaling, Danvers, MA, USA) in a dilution ratio of 1:1,000 at 4°C for 12 h, incubated with goat anti-rabbit IgG H+L (horseradish peroxidase) (Abcam) in a dilution ratio of 1:2,000 at 25°C for 1.5 h, enriched with enhanced

chemiluminescence (ECL; for anti-GAPDH, GE Healthcare) and select ECL (for anti-p-TrkA, GE Healthcare) for 1 min, and visualized using a Luminescence Image Analysis System (Fujifilm, Tokyo, Japan). The level of protein bands in the lanes was quantified using ImageJ software (version 1.50, National Institutes of Health, Bethesda, MD, USA).

Immunochemical staining of NGF-SM-ApoE-LIP and SK-N-MC cells

The staining experiments for SK-N-MC cells were analogous to those for HBMECs described in the "Immunochemical staining of NGF-SM-ApoE-LIP and HBMECs" section. The differences between the two systems were the addition of NGF-SM-ApoE-LIP associated with 10 μM fibrillar $A\beta_{1\text{-}42}$ and the staining with anti-Aβ monoclonal antibody (Abcam) in a dilution ratio of 1:400 for SK-N-MC cells.

Influence of NGF-SM-ApoE-LIP on the brain of AD rats

Male Wistar rats (250–280 g, BioLasco, Taipei, Taiwan) at 8 weeks were raised with sanitized food and water in the Animal Laboratory of National Chung Cheng University in accordance with the guidelines of Institutional Animal Care and Use Committee. In addition, the animal experiments followed the Affidavit of Approval of Animal Use Protocol approved by the Institutional Animal Care and Use Committee of National Chung Cheng University. Seven rats were in an experimental group to study the impact of $A\beta_{1\text{-}42}$ and NGF-SM-ApoE-LIP on the brain. The rats were fasted for 12 h, treated with 0.4 mg/mL atropin (Hebei Depond Animal Health Technology, Hebei, People's Republic of China) by intraperitoneal (IP) injection at a dose of 0.4 mg/kg for 3 min, and anesthetized with 60 mg/mL sodium pentobarbital (Siegfried, Taoyuan, Taiwan) of 60 mg/mL by IP injection at a dose of 60 mg/kg. The lambda and bregma regions of the brain defined the anteroposterior (AP), mediolateral (ML), and dorsoventral (DV) domains. Based on the AP, ML, and DV points, a subtraction of 0.35 cm, 0.2 cm, and 0.27 cm yielded the subfield location of cornu ammonis area 1 (CA1) in the hippocampus. 3.3 mg/mL of fibrillar $A\beta_{1\text{-}42}$ was administered to the drilled DV domain by injection with 15 μL of final volume (flow rate of 2 μL/min for 7.5 min). The surgical cuts on the heads of rats were stitched, and then the rats were housed for 1 week before they were euthanized. Thus, the rat model of AD was established. For AD treatment, the suspension of free NGF (17.135 ng/mL), NGF-LIP (2 mg/mL), or NGF-SM-ApoE-LIP (2 mg/mL) was injected with 1 mL of total volume via tail vein. For intravenous injection purpose, the following sterilization techniques were used: exposure of needles to UV light, disinfection of the needles, cleaning the area of the skin with ethanol-soaked cotton before injection, and hemostasis of the injection area with ethanol-soaked cotton after injection. The treatment was carried out three times every 2 days.

MDA and AChE assay of brain tissue after treating with NGF-SM-ApoE-LIP

After the animals were euthanized, the homogenized hippocampal CA1 (10 mg) was immersed in 300 μL of lysis buffer (Abcam) and 3 μL of butylated hydroxytoluene (Abcam) and centrifuged at 12,000× *g* at 4°C for 5 min. To determine the MDA level in the hippocampus, L_{MDA} (MDA nmol/mg tissue), 50 μL of the supernatant in a 96-well plate was allowed to react with 150 μL of thiobarbituric acid (Abcam) at 95°C for 1 h and analyzed using the ELISA spectrophotometer at 532 nm at 25°C with calibration of the MDA standard (Abcam). In addition, the homogenized hippocampal CA1 (5 mg) was treated with 100 μL of lysis buffer (Abcam), 100 μL of tissue protein extraction reagent (Thermo Fisher Scientific), and 1 μL of Halt protease inhibitor cocktail (Thermo Fisher Scientific) and centrifuged at 2,000× *g* at 4°C for 10 min. To determine the AChE activity in the hippocampus, A_{AChE} (mU/mg tissue), 50 μL of the supernatant in a 96-well plate was treated with 50 μL of acetylthiocholine (Abcam) and 50 μL of 0.1% bovine serum albumin (BSA; Abcam) at 25°C for 30 min and analyzed using the ELISA spectrophotometer at 410 nm with calibration of the AChE standard (Abcam) and 0.1% BSA.

Nissl staining of the hippocampus after treating with NGF-SM-ApoE-LIP

The brain samples were hardened on dry ice, wrapped in tissue-tek optimal cutting temperature compound (Sakura Finetek, Torrance, CA, USA), and placed in an ultralow temperature freezer (Panasonic Healthcare, Gunma, Japan) at −80°C for 30 min. The hippocampal CA1 was sliced using a cryostat microtome (Leica, Wetzlar, Germany) at −20°C to obtain 10 μm thin tissue sections; the sections were then immersed in acetone (JT Baker) for 5 min, blocked with 0.1% (v/v) hydrogen peroxide (Sigma-Aldrich) in methanol (Mallinckrodt Baker, Phillipsburg, NJ, USA) for 1 min, treated with casein-based blocking reagent (Invitrogen, Waltham, MA, USA) for 1 h, incubated in 75% ethanol (Tedia, Fairfield, OH, USA) at 37°C for 8 h, treated with 0.1% (w/v) thionin (Sigma-Aldrich) for 20 min, submerged in 150 μL of acetic acid (Sigma-Aldrich) in 100 mL of 95%

ethanol for 2 min, dehydrated in ethanol with increasing concentration, immersed in o-xylene (Fluka, Buchs, Switzerland) for 3 min, and maintained in Entellan® new mounting medium (Millipore). Neuronal distribution in the hippocampus was then assessed using an inverted microscope (Nikon, Tokyo, Japan).

Statistics

Data are presented as mean ± standard deviation. The significant difference between groups of data was evaluated using a one-way analysis of variance followed by Tukey's HSD test.

Results and discussion

Physicochemical property of NGF-SM-ApoE-LIP

Particle size, surface charge, and morphology of NGF-SM-ApoE-LIP

Figure 1 shows the particulate characteristics of NGF-SM-ApoE-LIP. Figure 1A demonstrates the average particle diameter and zeta potential with insets displaying the corresponding SEM images. As indicated in the figure, an increase in the weight percentage of CL enlarged the average size of NGF-SM-ApoE-LIP from 115.1±6.1 nm to 154.4±4.1 nm. This was because the two phosphoric head groups of CL repelled each other, while the two tails of CL extended the bilayer. In addition, NGF-SM-ApoE-LIP carried a negative charge. An increase in the weight percentage of CL increased the absolute value of zeta potential of NGF-SM-ApoE-LIP. This is because CL is an anionic phospholipid that principally exists in the mitochondrial inner membrane for electron transport.[18] As exhibited in the insets of Figure 1A, the particle diameter of the spheroid-shaped particles was consistent with the data obtained. These SEM images were similar to the morphology of liposomes comprising phospholipids and cholesterol.[19] Figure 1B shows the TEM images of NGF-SM-ApoE-LIP. The grafting of SM and/or ApoE produced the dark exterior of these colloids. When both SM and ApoE were modified on NGF-SM-ApoE-LIP (Figure 1B[c]), a relatively dark particle was obtained because the covered surface moiety showed strong negative stains. Figure 1B also suggested that the structure of NGF-SM-ApoE-LIP could be completely integrated with bioactive SM and/or ApoE on the periphery. In this study, LIP was shown encapsulate hydrophilic NGF in the aqueous core. The entrapment efficiency of NGF was 34.27%±3.46% (n=3), which was a reasonable value of NGF confinement, and this can be potent dosage for applying to an AD model.[20] It was also observed that the surface properties of liposomes, such as particle size, surface area, and membrane rigidity, might affect the encapsulation of hydrophilic pharmaceuticals.[21] Moreover, the leakage of NGF from lipid bilayer was minor, in general, and the enclosed NGF could maintain its bioactivity and dodge the external interference when LIP was administered in a physiological milieu.[22]

Grafting efficiency of SM and ApoE on NGF-LIP

Figure 1C shows the grafting efficiency of SM and ApoE. As indicated in this figure, the effect of the quantity of CL on the variation in the grafting efficiency was insignificant. Two opposing influences might contribute to this outcome. First, an increase in the weight percentage of CL increased the diameter of NGF-SM-ApoE-LIP (shown in Figure 1A), leading to an augmented surface area on a particle and a reduced steric repulsion between competitive SM (or ApoE) for the grafting sites. Second, the negative surface charge on NGF-SM-ApoE-LIP increased with an increasing weight percentage of CL (shown in Figure 1A) and repelled the approaching of negatively charged SM and ApoE. As can be seen from Figure 1C, the grafting efficiency of SM was higher than that of ApoE. This was because the molecular size of SM was smaller than that of ApoE. Thus, the former experienced a smaller steric repulsion than the latter during cross-linking. In a study on the detoxification activity of membrane-bound glutathione transferase, it has been shown that CL-incorporated bilayers could embed a portion of the enzyme to form an electron-transport complex.[23]

Surface atom on NGF-SM-ApoE-LIP

Figure 1D shows the XPS spectra of NGF-SM-ApoE-LIP. The peaks at 283, 399, and 531 eV are, respectively, the signals of surface carbon, nitrogen, and oxygen. As indicated in Figure 1D, strong carbon and oxygen signals were detected. This was because carbon and oxygen were ample in the current particles comprising mainly phospholipid, large protein, and small peptide. In addition, the signals at 131 eV denoted the existence of phosphorus, attributing to the incorporation of DPPC, SPC, CL, and DSPE-PEG(2000)-CA on NGF-SM-ApoE-LIP. As revealed in spectrum (a) and (b), an increase in the weight percentage of CL procured a minor effect on the atomic signals. This resulted from the fact that the atomic components of CL are similar to those of other main ingredients used in the preparation. As can be seen in spectrum (c), an increase in the concentration of ApoE from 0 to 40 μg/mL slightly enhanced the nitrogen peak of NGF-ApoE-LIP, suggesting the association with ApoE, which contains

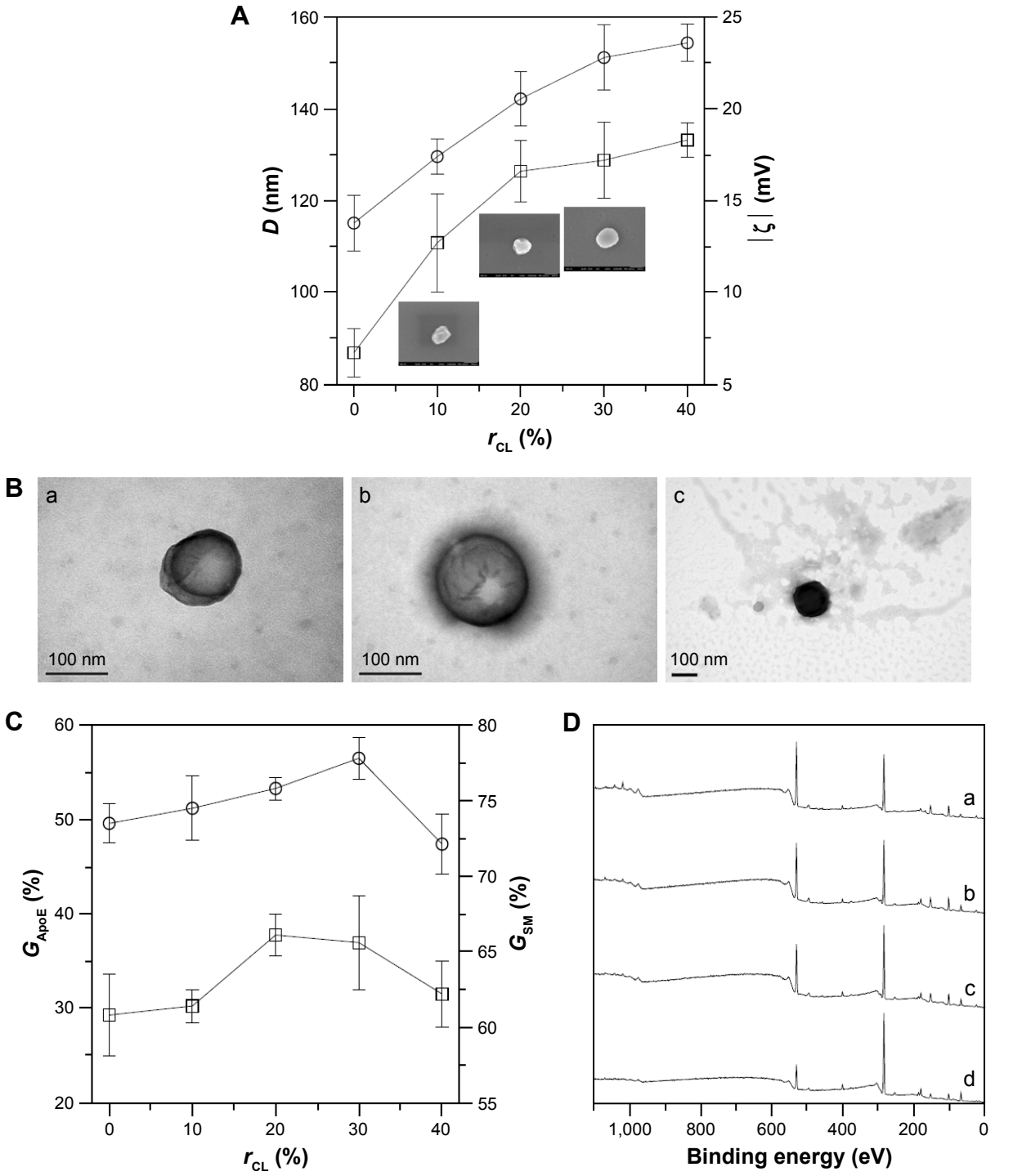

Figure 1 Physicochemical characterization of NGF-SM-ApoE-LIP.

Notes: (**A**) Average particle diameter and zeta potential; C_{SM} =40 μg/mL; C_{ApoE} =40 μg/mL; (○) average particle diameter; n=3; (□) zeta potential; n=3; inset: corresponding SEM images at r_{CL} =10%, r_{CL} =20%, r_{CL} =30%, (**B**) TEM images; r_{CL} =30%; (a) NGF-ApoE-LIP; C_{ApoE} =40 μg/mL; (b) NGF-SM-LIP; C_{SM} =40 μg/mL; (c) NGF-SM-ApoE-LIP; C_{SM} =40 μg/mL; C_{ApoE} =40 μg/mL, (**C**) grafting efficiency; (○) grafting efficiency of ApoE on NGF-LIP; C_{SM} =0 μg/mL; n=3; (□) grafting efficiency of SM on NGF-ApoE-LIP; C_{ApoE} =40 μg/mL; n=3, (**D**) XPS spectra; (a) NGF-LIP; r_{CL} =0%; (b) NGF-LIP; r_{CL} =30%; (c) NGF-ApoE-LIP; r_{CL} =30%; C_{ApoE} =40 μg/mL; (d) NGF-SM-ApoE-LIP; r_{CL} =30%; C_{SM} =40 μg/mL; C_{ApoE} =40 μg/mL.

Abbreviations: C_{SM}, concentration of serotonin modulator; C_{ApoE}, concentration of apolipoprotein E; r_{CL}, weight percentage of cardiolipin in bilayer (%).

abundant amino acids. The spectrum (d) demonstrated that the grafting of SM also promoted the nitrogen peak. Figure 1D was consistent with the TEM images (shown in Figure 1B) and the grafting efficiency of ApoE and SM (shown in Figure 1C). Moreover, the modifications of ApoE and SM reduced the oxygen signal. This was because surface ApoE and SM could partially cover the oxygen-containing groups, such as C-O-C and O-C=O, on NGF-SM-ApoE-LIP.

Transport of NGF-SM-ApoE-LIP across the BBB

Cytotoxicity of NGF-SM-ApoE-LIP to the BBB cells

Figure 2 shows the transport behavior of NGF-SM-ApoE-LIP across the BBB. Figure 2A shows the viability of HBMECs and HAs after treating with NGF-SM-ApoE-LIP. As indicated in this figure, NGF-SM-ApoE-LIP was only very slightly toxicity to the BBB cells. The differences in the cell viability (as seen in Figure 2A) were not significant. This was because the lipid ingredients, targeting molecules, and NGF had high biocompatibility. In addition, the negative charge of NGF-SM-ApoE-LIP was electrically repulsive to the negative charge of mammalian cells, conducive to a mild interaction during particle internalization, which increased the viability.[24,25] However, NGF-SM-ApoE-LIP might cause lipid fusion with cell membrane and provoke a slight inflammatory response.[26–28] Based on Figure 2A, NGF-SM-ApoE-LIP did not apparently jeopardize HBMECs and HAs when delivering NGF across the BBB.

Effect of NGF-SM-ApoE-LIP on the BBB permeability of NGF

Figure 2B shows the influence of NGF-SM-ApoE-LIP on the integrity of HBMEC/HA. As indicated in this figure, the

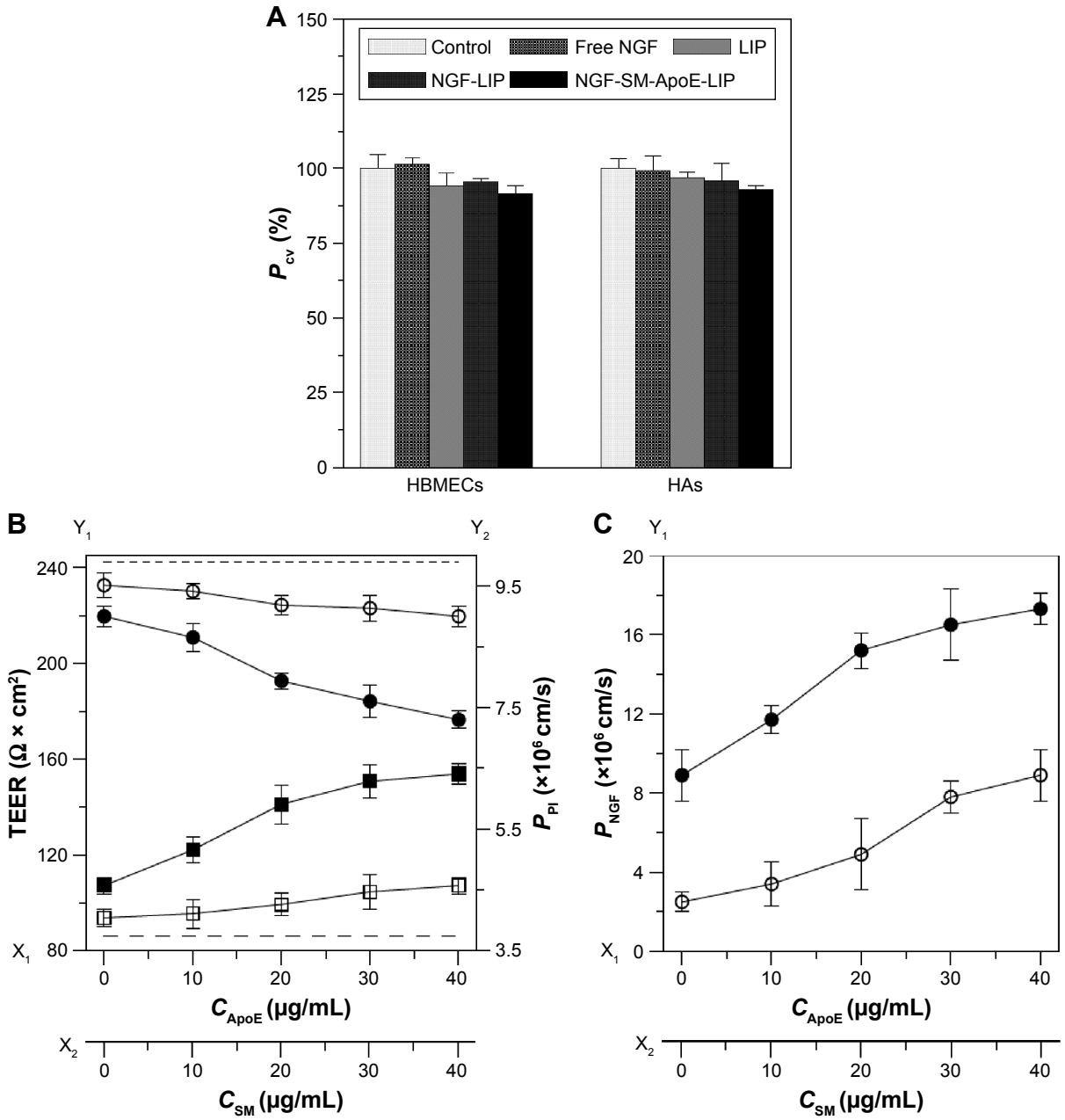

Figure 2 (*Continued*)

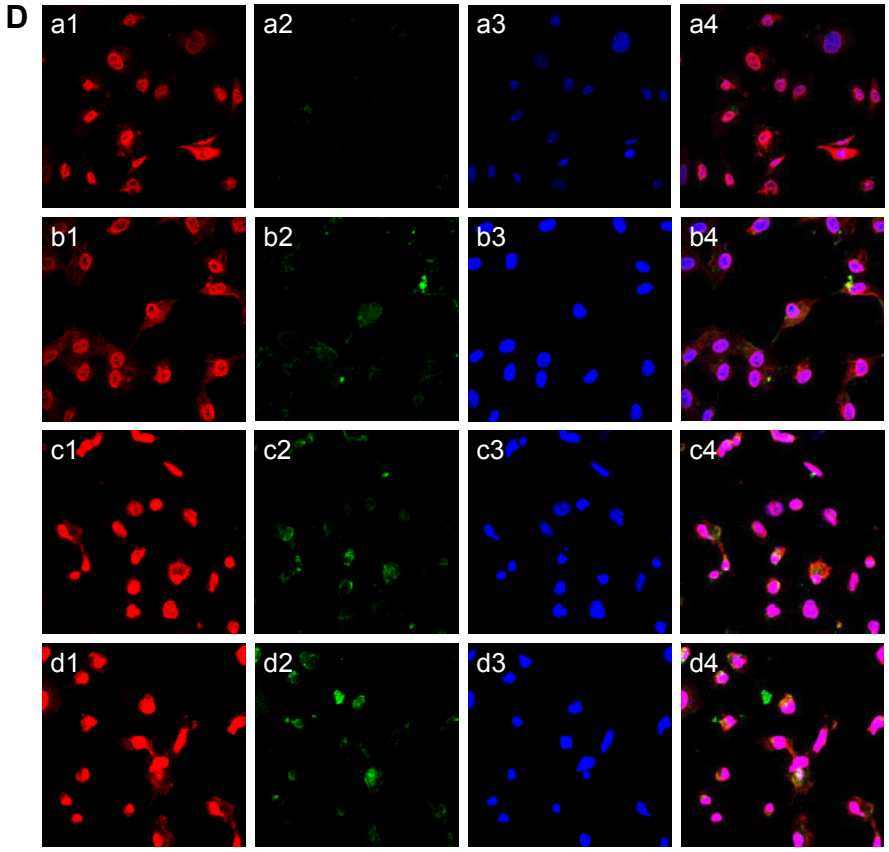

Figure 2 Effect of NGF-SM-ApoE-LIP on the BBB permeation.

Notes: r_{CL} =30%. (**A**) Viability of HBMECs and HAs; C_{SM} =40 μg/mL; C_{ApoE} =40 μg/mL; n=3, (**B**) TEER and permeability coefficient of PI across HBMEC/HA; (○) TEER; NGF-ApoE-LIP; (X_1 and Y_1 axes); (●) TEER; NGF-SM-ApoE-LIP; C_{ApoE} =40 μg/mL; X_2 and Y_1 axes; (- - -): intact TEER; Y_1 axis; n=3, (□) permeability coefficient of PI; NGF-ApoE-LIP; X_1 and Y_2 axes; (■) permeability coefficient of PI; NGF-SM-ApoE-LIP; C_{ApoE} =40 μg/mL; X_2 and Y_2 axes; (– – –): intact permeability coefficient of PI; Y_2 axis; n=3, (**C**) permeability coefficient of NGF across HBMEC/HA; (○) NGF-ApoE-LIP; (●) NGF-SM-ApoE-LIP; C_{ApoE} =40 μg/mL; n=3, (**D**) fluorescent NGF-SM-ApoE-LIP internalized by HBMECs; C_{ApoE} =40 μg/mL; (a) NGF-LIP; (b) NGF-ApoE-LIP; (**c**) NGF-SM-ApoE-LIP; C_{SM} =20 μg/mL; (d) NGF-SM-ApoE-LIP; C_{SM} =40 μg/mL; (a1, b1, c1, d1), (a2, b2, c2, d2), (a3, b3, c3, d3), and (a4, b4, c4, d4) are red (against LDLR antibody in [a] and [b] and against both LDLR and SR antibody in [c] and [d]), green (LIP carrier), blue (DAPI for nucleus), and merged channels, respectively. a1, a2, and a3 are obtained from excitation at 555 nm, 490 nm, and 350 nm, respectively. a4 is a merged image from a1–a3. The difference between a1–a4 is the same for b, c, and d.

Abbreviations: r_{CL}, weight percentage of cardiolipin in bilayer (%); C_{SM}, concentration of serotonin modulator; C_{ApoE}, concentration of apolipoprotein E; HBMEC, human brain-microvascular endothelial cell; HA, human astrocyte; BBB, blood–brain barrier; TEER, transendothelial electrical resistance; LIP, liposome; SM, serotonin modulator; NGF, nerve growth factor.

administration of NGF-SM-ApoE-LIP reduced the TEER and enhanced the permeability coefficient of PI across the BBB (P_{PI}), suggesting a temporary deterioration of the tight junction. An increase in the concentration of ApoE and SM decreased the TEER and increased the permeability coefficient of PI. This was because ApoE and SM promoted the binding of NGF-SM-ApoE-LIP with LDLR and SR on HBMECs, respectively. Thus, the tight junction connecting actin bundles was partially disturbed.[29,30] In a study on the opening of tight junction using digital holographic microscopy for quantitative phase images, the tight junction, after interacting with chitosan nanoparticles, was opened at 3 h and 9 h and closed at 17 h, while TEER decreased and then increased.[31] In addition, it has been observed that the compactness of the tight junction could be preserved by the use of NGF-encapsulated liposomes.[22] The data in Figure 2B suggested an adequate tight junction and a sound linkage of the BBB after treatment with NGF-SM-ApoE-LIP. Hence, the permeability coefficient of NGF could first be evaluated in this cell model before in vivo targeting delivery of NGF-SM-ApoE-LIP. Figure 2C shows the permeability coefficient of NGF across HBMEC/HA using NGF-SM-ApoE-LIP. As indicated in this figure, an increase in the concentration of ApoE and SM increased the permeability coefficient of NGF. When the concentration of both ApoE and SM was 40 μg/mL, NGF-SM-ApoE-LIP increased the permeability coefficient of NGF about 8 times the corresponding value of NGF-LIP. Thus, NGF-SM-ApoE-LIP could be a potent targeting carrier to transport NGF across the BBB. An efficient delivery of medicinal substance across the BBB is not a common physiological phenomenon. It has been shown that hydrophobic drugs and molecules with molecular weights less 400 Da can cross the BBB.[32] Based on this general principle, free NGF is not capable of crossing the BBB as it is a hydrophilic protein with molecular weight of 27 kDa.[33,34] Thus,

the use of surface modification with functional biomolecules can be an efficacious strategy for NGF to cross the BBB.[35] The use of transferrin and p-aminophenyl-α-D-manno-pyranoside in LIP carriers, for example, could accelerate the mass transport across endothelial cells.[36] After traversing HBMEC/HA, the majority of NGF-SM-ApoE-LIP will be intact particles, although a minor portion of NGF could escape from the carriers in the donor chamber and/or in HBMECs.

Fluorescent image of NGF-SM-ApoE-LIP and expressed SR and LDLR

Figure 2D shows the images of immunochemical staining for the uptake of NGF-SM-ApoE-LIP by HBMECs via expressed LDLR and/or SR. The red, blue, and green stains were receptors, nuclei, and drug carriers, respectively. The yellow marks indicate superimposition of red and green stains. The green, red, and blue stains merged into the white spots. As indicated in Figure 2D(a), a few green stains near and on HBMECs were observed, revealing a nonspecific interaction, including nanostructure affinity and/or lipid binding to NGF-LIP for membrane fusion.[37] As can be seen in Figure 2D(b), NGF-ApoE-LIP could be endocytosed by HBMECs. This suggested that the modified ApoE was recognized by LDLR on HBMECs and enabled permeation across the BBB. When compared with Figure 2D(b), Figure 2D(c) demonstrated a much higher green staining intensity. This was because the camouflage of both SM and ApoE on the surface elicited receptor-mediated endocytosis and promoted the internalization of NGF-SM-ApoE-LIP by HBMECs. In addition, the prevalent conjugation of SM with SR and ApoE with LDLR could be observed. As exhibited in Figure 2D(d), the green intensity reached the highest level in this study. This suggested an extensive uptake and effectual transcytosis to carry NGF across HBMECs. Moreover, the images shown in Figure 2D were consistent with the data presented in Figure 2B and C. Figure 2D(a) and 2D(b) evidenced abundant LDLR on the membrane of HBMECs. It has been found that LDLR was also highly expressed on bovine, rat, and marmoset brain endothelia.[38,39] In addition to LDLR, the intensity of red staining in Figure 2D(c) and 2D(d) was stronger than that in Figure 2D(a) and 2D(b), suggesting that HBMECs could express quite a few SR. This expression is consistent with previous literature.[40]

Interaction of NGF-SM-ApoE-LIP with degenerated SK-N-MC cells

Rescue of SK-N-MC cells by NGF-SM-ApoE-LIP

Figure 3A shows the viability of SK-N-MC cells treated with NGF-SM-ApoE-LIP. As indicated in this figure, insult with $A\beta_{1-42}$ evidently decreased the viability of SK-N-MC cells owing to its strong neurotoxicity. The order of viability was NGF-SM-ApoE-LIP > NGF-LIP > NGF. Three reasons could be responsible for this order. First, free NGF was sensitive to the microenvironment and could be degraded rapidly and lose its activity in the medium. Second, the affinity of CL to $A\beta_{1-42}$ was high.[41] Thus, the incorporation of CL in the lipid bilayer of NGF-LIP enhanced the viability by localized release of NGF around SK-N-MC cells. With regard to the attraction for $A\beta_{1-42}$, it has been found that a use of AA3E2 could decrease the cytotoxicity to SK-N-MC cells because of the high affinity of AA3E2 to $A\beta_{1-42}$.[42] In addition to the targeting effect, the addition of CL in lipids could stabilize the bilayer and appreciably reduce the water permeation through LIP.[43] Third, surface ApoE could target LDLR to prevent SK-N-MC cells from $A\beta_{1-42}$-inuced neurodegeneration.

Expression of p-TrkA by SK-N-MC cells after treating with NGF-SM-ApoE-LIP

Figure 3B shows the Western blot of p-TrkA and GAPDH and the ratio of the two proteins in the solution of ruptured SK-N-MC cells. As indicated in this figure, the amount of p-TrkA expressed by the $A\beta_{1-42}$ group (AD model) reduced when compared with the control group. This suggested that the neurodegeneration of SK-N-MC cells was more widespread than the resistance to the insult with $A\beta_{1-42}$ for survival. In a study on TrkA pathway, $A\beta_{1-42}$ was found to mediate the signaling cascades relevant to the TrkA expression.[44] In addition, the dysfunction of TrkA could be the most essential cause of neurodegeneration in the end stage of AD.[45] Moreover, the oder of the quantity of p-TrkA was NGF-SM-ApoE-LIP > NGF-LIP > NGF, which was the same as that for the viability of SK-N-MC cells (shown in Figure 3A). The rationale behind this outcome could be due to the following reasons. NGF could rescue SK-N-MC cells from apoptosis via upregulating the signaling of endogenous TrkA. However, free NGF might be deactivated in the culture medium. NGF-LIP could prevent free NGF from rapid deactivation and maintain continuous delivery of NGF to the medium close to SK-N-MC cells. Therefore, the capacity of NGF-LIP to stimulate the expression of p-TrkA was stronger than that of free NGF. Moreover, NGF-SM-ApoE-LIP triggered the targeting characteristics for receptor-mediated endocytosis, leading to a promoted uptake and a focal release of NGF to nourish SK-N-MC cells.

Binding of NGF-SM-ApoE-LIP to $A\beta_{1-42}$ and SK-N-MC cells

Figure 3C shows the fluorescent images of NGF-SM-ApoE-LIP and $A\beta_{1-42}$-enclosed SK-N-MC cells. As seen in this figure, LIP carriers (stained green) could interact with SK-N-MC cells (stained blue) and attach to $A\beta_{1-42}$. $A\beta_{1-42}$ (stained red) next to the nuclei was manifested as satellite deposits in the neighborhood of SK-N-MC cells. As can be seen in Figure 3C(a), NGF-LIP could adhere to SK-N-MC cells owing to lipid affinity. Figure 3C(b) shows that the accumulated $A\beta_{1-42}$ was attractive to NGF-LIP. This was because CL in NGF-LIP could bind to $A\beta_{1-42}$ for deposition of carriers adjacent to SK-N-MC cells. As demonstrated in Figure 3C(c), NGF-SM-LIP had no particular capacity to recognize SK-N-MC cells. In addition, the quantity of yellow (from green and red) and white (from green, red, and blue) dots in Figure 3C(d) were more than that in Figure 3C(c), evidencing a better docking of NGF-SM-ApoE-LIP to $A\beta_{1-42}$ and SK-N-MC cells. This intensified interaction could be attributed to the following two reasons. First, SK-N-MC cells expressed abundant LDLR and low-density lipoprotein receptor-related protein (LRP) to conjugate ApoE on NGF-SM-ApoE-LIP for enhanced cell penetration.[17] Second, it has been found that the ligands of LRP also existed in Aβ plaques of AD patients.[46] It has also been observed that the cognitive function of aged rats was improved by associating SM with SR.[47] Since surface ApoE can salvage SK-N-MC cells from the insult with $A\beta_{1-42}$, the effect of NGF-SM-ApoE-LIP on SK-N-MC cells was highlighted in this study.[48] Therefore, NGF-SM-ApoE-LIP could be localized around SK-N-MC

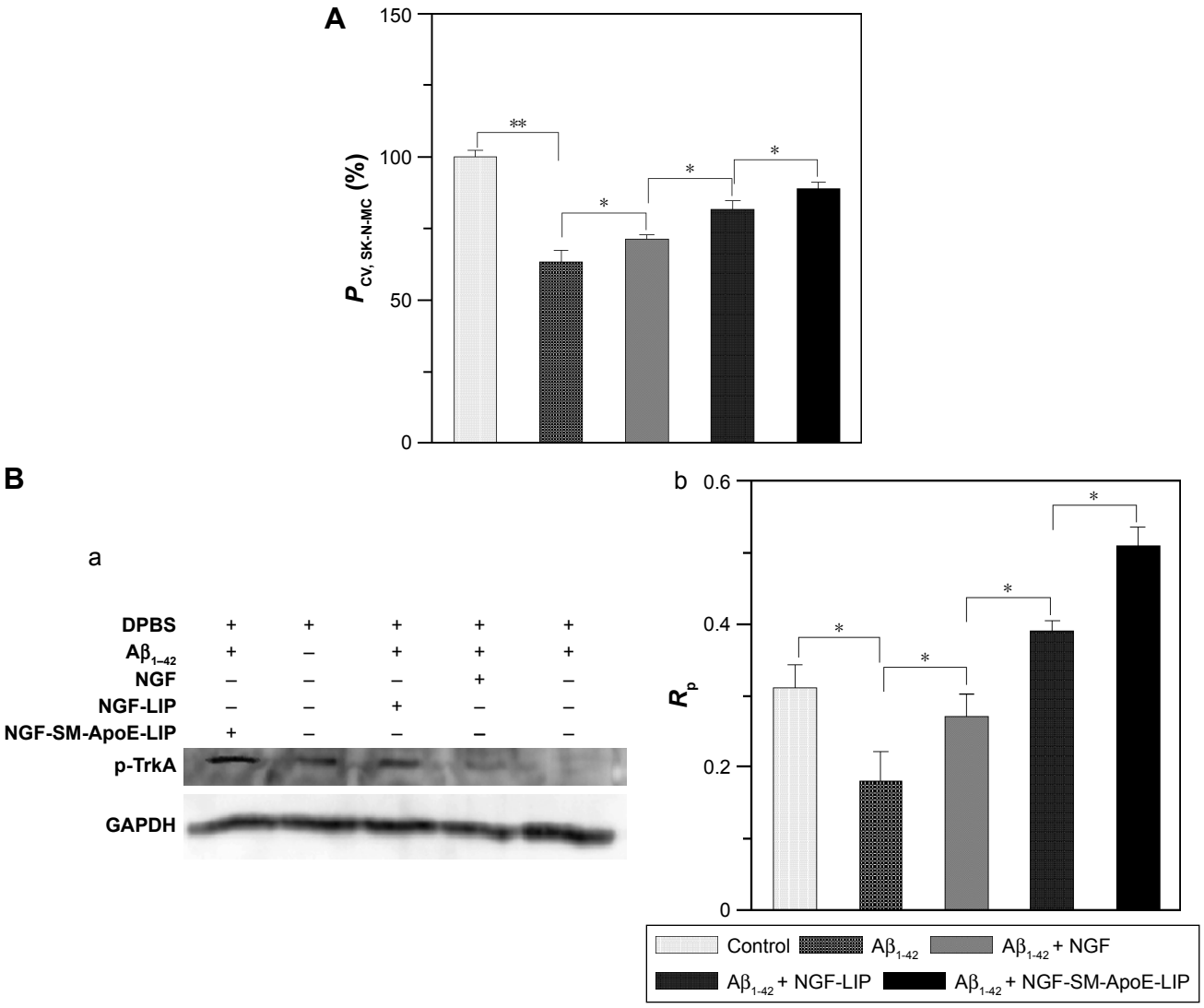

Figure 3 (*Continued*)

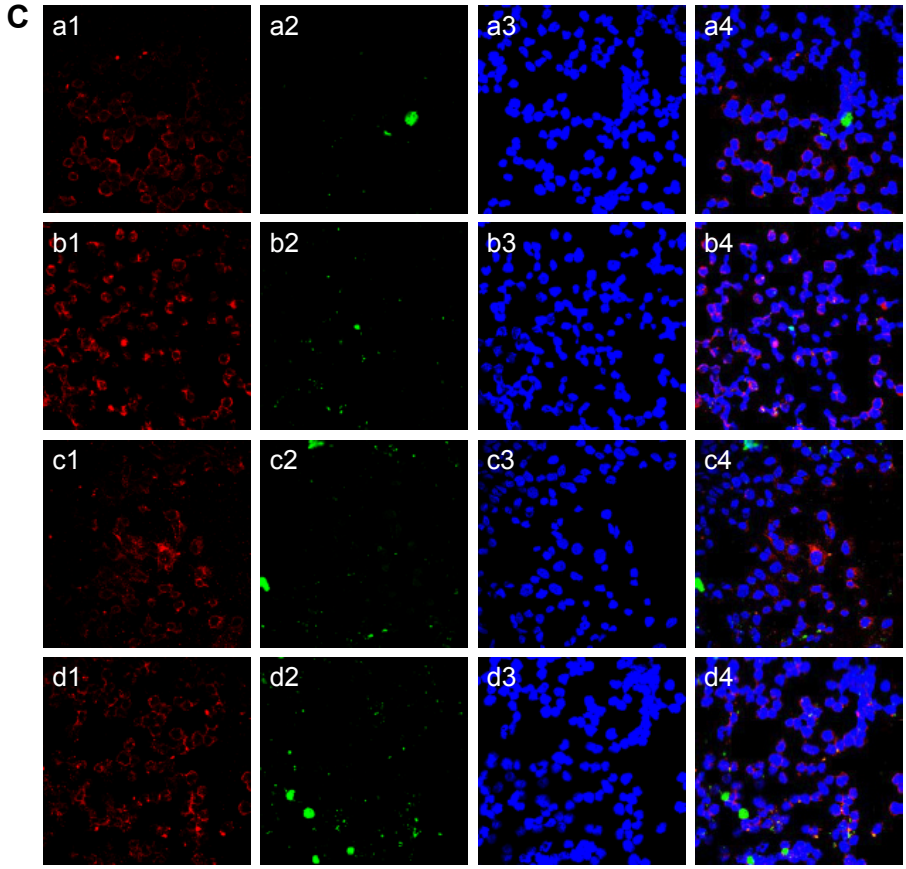

Figure 3 Effect of NGF-SM-ApoE-LIP on the survival of neurons treated with $A\beta_{1-42}$. C_{SM} =40 μg/mL; C_{ApoE} =40 μg/mL.
Notes: (A) Viability of SK-N-MC cells; r_{CL} =30%; *P<0.05; **P<0.01; n=3, (**B**) p-TrkA level of SK-N-MC cells; r_{CL} =30%; (a): Western blot; (b): R_p, *P<0.05; n=3, (**C**) immunochemical staining images of NGF-SM-ApoE-LIP interacting with SK-N-MC cells; (a) NGF-LIP; r_{CL} =0%; (b) NGF-LIP; r_{CL} =30%; (c) NGF-SM-LIP; r_{CL} =30%; (d) NGF-SM-ApoE-LIP; r_{CL} =30%; (a1, b1, c1, d1), (a2, b2, c2, d2), (a3, b3, c3, d3), and (a4, b4, c4, d4) are red (against $A\beta_{1-42}$ antibody), green (LIP carrier), blue (DAPI for nucleus), and merged channels, respectively. a1, a2, and a3 are obtained from excitation at 555 nm, 490 nm, and 350 nm, respectively. a4 is a merged image from a1–a3. The difference between a1–a4 is the same for b, c, and d.
Abbreviations: C_{SM}, concentration of serotonin modulator; C_{ApoE}, concentration of apolipoprotein E; r_{CL}, weight percentage of cardiolipin in bilayer (%); R_p, protein ratio of p-TrkA to GAPDH; LIP, liposome; SM, serotonin modulator; NGF, nerve growth factor.

cells treated with $A\beta_{1-42}$ for topical delivery and promote the activity of NGF to inhibit neuronal apoptosis. Figure 3C was consistent with the results observed in Figure 3A and B.

NGF-SM-ApoE-LIP for AD treatment in vivo

Biochemical assessment of brain tissue after treating with NGF-SM-ApoE-LIP

Figure 4 shows the therapeutic outcome of the treatment with NGF-SM-ApoE-LIP in rats with memory deficit. Figure 4A shows the MDA level in the hippocampal CA1. As shown in this figure, the MDA level of the $A\beta_{1-42}$ group was significantly higher than that of the control group (sham). The synthesis of MDA in the hippocampus demonstrated the features of lipid peroxidation owing to the attack of free radicals on AD brain tissue.[49] The high MDA level of the $A\beta_{1-42}$ group represented a strong oxidative stress preceding other neuropathological conditions in the brain.[50,51] The treatment with free NGF through the circulation system did not appreciably reduce the MDA level in the $A\beta_{1-42}$ group, suggesting a decrease in the activity of NGF to hamper the production of MDA-protein adducts in the brain. The order of the MDA level was NGF > NGF-LIP > NGF-SM-ApoE-LIP. This result was consistent with the in vitro study on SK-N-MC cells (shown in Figure 3). It is worth noting that surface DSPE-PEG(2000) could prolong the circulation of NGF-SM-ApoE-LIP in the blood via steric stabilization, reduce the elimination of the particles by the reticuloendothelial system, and eschew the conjugation with plasma opsonin. In addition, the leakage of NGF from NGF-SM-ApoE-LIP could be negligible during penetration of the BBB. It has been found that the percentage of NGF released from LIP to the blood was less than 10% for 4 h.[22] Figure 4B shows the AChE activity in the CA1 of AD rat brains. A high AChE activity implied

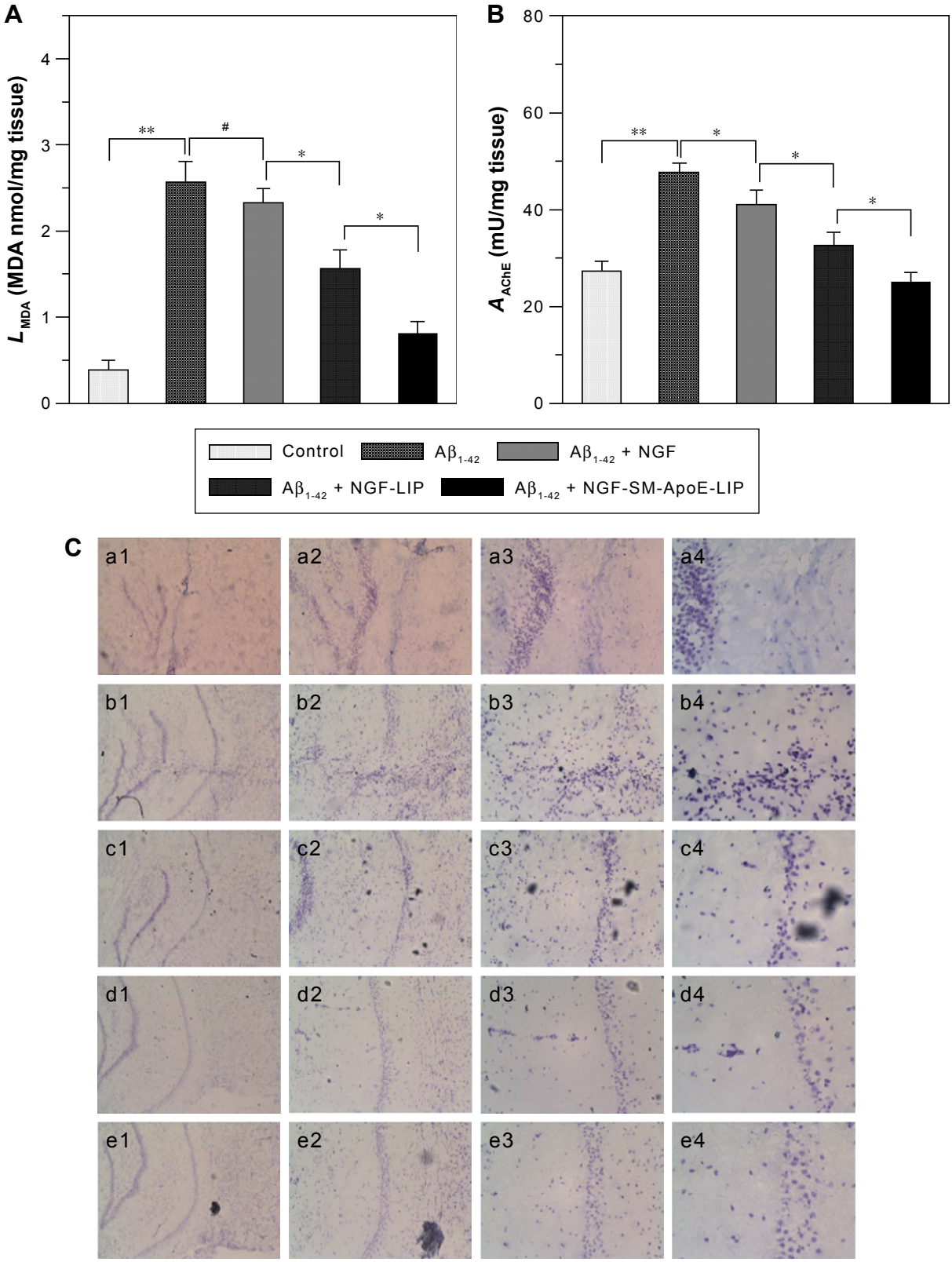

Figure 4 Biochemical analysis and histochemical staining of the brain of AD rats treated with NGF-SM-ApoE-LIP. r_{CL} =30%; C_{SM} =40 μg/mL; C_{ApoE} =40 μg/mL.

Notes: (**A**) MDA level of the brain CA1 tissue after treating with LIP nanocarriers; *$P<0.05$; #$P>0.05$; **$P<0.01$; n=6, (**B**) AChE activity of the brain CA1 tissue after treating with LIP nanocarriers; (a) control; (b) $A\beta_{1-42}$; (c) $A\beta_{1-42}$ + NGF; (d) $A\beta_{1-42}$ + NGF-LIP; (e) $A\beta_{1-42}$ + NGF-SM-ApoE-LIP; (a1, b1, c1, d1, e1) 40×; (a2, b2, c2, d2, e2) 100×; (a3, b3, c3, d3, e3) 200×; (a4, b4, c4, d4, e4) 400×. a1, a2, a3, and a4 were obtained from magnification at 40×, 100×, 200×, and 400×, respectively. The difference between a1–a4 is the same for b, c, d, and e.

Abbreviations: r_{CL}, weight percentage of cardiolipin in bilayer (%); C_{SM}, concentration of serotonin modulator; C_{ApoE}, concentration of apolipoprotein E; LIP, liposome; SM, serotonin modulator; NGF, nerve growth factor; MDA, malondialdehyde.

a rapid decay of acetylcholine. Thus, the AChE activity could be closely connected to the nervous peroxidation and Aβ aggregation.[52,53] As can be seen in Figure 4B, the AChE activity of the $A\beta_{1-42}$ group was significantly higher than that of the control group, suggesting a strong toxicity of $A\beta_{1-42}$, leading to deactivation of the neurotransmission function. With regard to AChE activity, the efficacy of the formulations was NGF > NGF-LIP > NGF-SM-ApoE-LIP. It is worth noting that after induction with $A\beta_{1-42}$, NGF-SM-ApoE-LIP noticeably reduced the AChE activity to the average value of the control group, evidencing an active constraint on the production of AChE in the brain with accumulated $A\beta_{1-42}$.

Neuronal distribution in the hippocampus after treating with NGF-SM-ApoE-LIP

Figure 4C shows the fluorescent images of stained neurons in the hippocampus of AD rat brains. As can be seen in this figure, the purple dots are neurons, including normal, pathogenic, apoptotic, and dead cells. The typical appearance of living neurons is ellipsoidal, while dead neurons present sharp angles around the cell periphery. As shown in Figure 4C(b), insult with $A\beta_{1-42}$ reduced the percentage of living neurons in the hippocampus when compared with the control group (shown in Figure 4C[a]). Figure 4C(c–e) demonstrates that the three formulations could protect regular neurons against neurodegeneration in the CNS. Figure 4C(c) suggested the ability of free NGF to elicit neurotrophic actions in the CA1 and preserve active neurons from serious retrogression. As exhibited in Figure 4C(d), NGF-LIP could considerably subserve the nervous survival. In addition, the treatment with NGF-SM-ApoE-LIP could rescue neurons from apoptosis and yield the best recovery of living neurons from the injured brain (Figure 4C[e]). Thus, the capacity of targeting to the BBB (SM and ApoE), conjugation with $A\beta_{1-42}$ (CL), and neural recognition (ApoE) enabled NGF-SM-ApoE-LIP to effectively deliver NGF for AD therapy. It has been observed that SM might enhance the dopamine levels by desensitization of SR on dopamine terminals.[54] Moreover, cholesterol complexed to ApoE-containing lipoproteins could promote synaptogenesis and synaptic connections.[55] In a study on the treatment for cerebral cortex lesions with *N*-methyl-*D*-aspartic acid, a systemic administration of NGF and OX-26 conjugate was able to protect cholinergic basal forebrain neurons against retrograde atrophy.[56]

Conclusion

Functional NGF-SM-ApoE-LIP was fabricated and characterized, and the BBB cells showed a high viability after treating with NGF-SM-ApoE-LIP. Modified SM and ApoE on the liposomal surface preserved bioactivity and played a crucial role in targeting the BBB, enabling high penetration of NGF-SM-ApoE-LIP across HBMEC/HA. In addition to a low cytotoxicity, NGF-SM-ApoE-LIP stimulated SK-N-MC cells to express p-TrkA and prevented these cholinergic neurons from apoptosis. Moreover, CL incorporated in the bilayer also favored the docking of NGF-SM-ApoE-LIP to neuron-surrounded $A\beta_{1-42}$, and ApoE on the carrier surface could recognize LDLR on SK-N-MC cells, resulting in inhibition of the neurotoxicity due to the deposited $A\beta_{1-42}$. Based on the ability to bind with the BBB and neurons, NGF-SM-ApoE-LIP substantially decreased the MDA level and AChE activity in the hippocampus of AD rats and retarded the degeneration of brain administered fibrillar $A\beta_{1-42}$. Thus, in vitro and in vivo evidences testified the potential of NGF-SM-ApoE-LIP as being suitable for use as a clinical neuroprotective agent in AD management.

Acknowledgments

This work is supported by the Ministry of Science and Technology of the Republic of China.

Disclosure

The authors report no conflicts of interest in this work.

References

1. Goedert M, Spillantini MG. A century of Alzheimer's disease. *Science*. 2006;314:777–781.
2. Alzheimer's Association. 2016 Alzheimer's disease facts and figures. *Alzheimers Dement*. 2016;12:1–79.
3. Obara Y, Yamauchi A, Takehara S, Niemoto W, Takahashi M, Stork PJ. ERK5 activity is required for nerve growth factor-induced neurite outgrowth and stabilization of tyrosine hydroxylase in PC12 cells. *J Biol Chem*. 2009;284:64–73.
4. Sofroniew MV, Howe CL, Mobley WC. Nerve growth factor signaling, neuroprotection, and neural repair. *Annu Rev Neurosci*. 2001;24:1217–1281.
5. Bottger D, Ullrich C, Humpel C. Monocytes deliver bioactive nerve growth factor through a brain capillary endothelial cell-monolayer in vitro and counteract degeneration of cholinergic neurons. *Brain Res*. 2010; 1312:108–119.
6. Eriksdotter-Jonhagen M, Nordberg A, Amberla K, et al. Intracerebroventricular infusion of nerve growth factor in three patients with Alzheimer's disease. *Dement Geriatr Cogn Disord*. 1998;9: 246–257.
7. Salt TE, Hill RG. Neurotransmitter candidates of somatosensory primary afferent fibres. *Neuroscience*. 1983;10:1083–1103.
8. Rouselle JC, Massot O, Delepierre M, Zifa E, Rosseau B, Fillion G. Isolation and characterization of an endogenous peptide from rat brain interacting specifically with the serotonergic 1B receptor subtypes. *J Biol Chem*. 1996;271:726–735.
9. Ullmer C, Schmuck K, Kalkman H, Lubbert H. Expression of serotonin receptor mRNAs in blood vessels. *FEBS Lett*. 1995;370: 215–221.
10. Re F, Cambianica I, Sesana S, et al. Functionalization with ApoE-derived peptides enhances the interaction with brain capillary endothelial cells of nanoliposomes binding amyloid-beta peptide. *J Biotechnol*. 2011; 156:341–346.

11. Wagner S, Zensi A, Wien SL, et al. Uptake mechanism of ApoE-modified nanoparticles on brain capillary endothelial cells as a blood–brain barrier model. *PLoS One*. 2012;7:e32568.
12. Mahley RW. Apolipoprotein E: cholesterol transport protein with expanding role in cell biology. *Science*. 1988;240:622–630.
13. LaDu MJ, Gilligan SM, Lukens JR, et al. Nascent astrocyte particles differ from lipoproteins in CSF. *J Neurochem*. 1998;70:2070–2081.
14. LaDu MJ, Shah JA, Reardon CA, et al. Apolipoprotein E and apolipoprotein E receptors modulate A beta-induced glial neuroinflammatory responses. *Neurochem Int*. 2001;39:427–434.
15. Kuo YC, Su FL. Transport of stavudine, delavirdine, and saquinavir across the blood–brain barrier by polybutylcyanoacrylate, methylmethacrylate–sulfopropylmethacrylate, and solid lipid nanoparticles. *Int J Pharm*. 2007;340:143–152.
16. Kuo YC, Lu CH. Effect of human astrocytes on the characteristics of human brain-microvascular endothelial cells in the blood–brain barrier. *Colloids Surf B Biointerfaces*. 2011;86:225–231.
17. Kuo YC, Wang CT. Protection of SK-N-MC cells against β-amyloid peptide-induced degeneration using neuron growth factor-loaded liposomes with surface lactoferrin. *Biomaterials*. 2014;35:5954–5964.
18. Klingenberg M. Cardiolipin and mitochondrial carriers. *Biochim Biophys Acta*. 2009;1788:2048–2058.
19. Yousefi A, Esmaeili F, Rahimian S, Atyabi F, Dinarvand R. Preparation and in vitro evaluation of a pegylated nano-liposomal formulation containing docetaxel. *Scientia Pharmaceutica*. 2009;77:453–464.
20. Kuo YC, Chou PR. Neuroprotection against degeneration of SK-N-MC cells using neuron growth factor-encapsulated liposomes with surface cereport and transferrin. *J Pharm Sci*. 2014;103:2484–2497.
21. Nii T, Ishii F. Encapsulation efficiency of water-soluble and insoluble drugs in liposomes prepared by the microencapsulation vesicle method. *Int J Pharm*. 2005;298:198–205.
22. Xie Y, Ye L, Zhang X, et al. Transport of nerve growth factor encapsulated into liposomes across the blood–brain barrier: in vitro and in vivo studies. *J Control Release*. 2005;105:106–119.
23. Shimoji M, Imaizumi N, Aniya Y. Modulation of membrane-bound glutathione transferase activity by phospholipids including cardiolipin. *Biol Pharm Bull*. 2011;34:209–213.
24. Muller RH, Maassen S, Weyhers H, Specht F, Lucks JS. Cytotoxicity of magnetite-loaded polylactide, polylactide/glycolide particles and solid lipid nanoparticles. *Int J Pharm*. 1996;138:85–94.
25. Kuo YC, Wang CC. Cationic solid lipid nanoparticles with primary and quaternary amines for release of saquinavir and biocompatibility with endothelia. *Colloids Surf B Biointerfaces*. 2013;101:101–105.
26. Jones CF, Grainger DW. In vitro assessments of nanomaterial toxicity. *Adv Drug Deliv Rev*. 2009;61:438–456.
27. Lin CH, Al-Suwayeh SA, Hung CF, Chen CC, Fang JY. Camptothecin-loaded liposomes with α-melanocyte-stimulating hormone enhance cytotoxicity toward and cellular uptake by melanomas: an application of nanomedicine on natural product. *J Tradit Complemen Med*. 2013;3:102–109.
28. Kuo YC, Chung JF. Physicochemical properties of nevirapine-loaded solid lipid nanoparticles and nanostructured lipid carriers. *Colloids Surf B Biointerfaces*. 2011;83:299–306.
29. Dejana E. Endothelial cell-cell junctions: happy together. *Nat Rev Mol Cell Biol*. 2004;5:261–270.
30. Kuo YC, Kuo CY. Electromagnetic interference in the permeability of saquinavir across the blood–brain barrier using nanoparticulate carriers. *Int J Pharm*. 2008;351:271–281.
31. Kaiser M, Pereira S, Pohl L, et al. Chitosan encapsulation modulates the effect of capsaicin on the tight junctions of MDCK cells. *Sci Rep*. 2015;5:10048.
32. Pardridge WM. Drug targeting to the brain. *Pharm Res*. 2007;24:1733–1744.
33. Hefti F. Is Alzheimer disease caused by lack of nerve growth factor? *Ann Neurol*. 1983;13:109–110.
34. Longo FM, Vu TK, Mobley WC. The in vitro biological effect of nerve growth factor is inhibited by synthetic peptides. *Cell Regulation*. 1990;1:189−195.
35. Friden PM, Walus LR, Watson P, et al. Blood–brain barrier penetration and in vivo activity of an NGF conjugate. *Science*. 1993;259:373–377.
36. Ying X, Wen H, Lua WL, et al. Dual-targeting daunorubicin liposomes improve the therapeutic efficacy of brain glioma in animals. *J Control Release*. 2010;141:183–192.
37. Duzgunes N, Nir S. Mechanisms and kinetics of liposome-cell interactions. *Adv Drug Deliv Rev*. 1999;40:3–18.
38. Dehouck B, Fenart L, Dehouck MP, Pierce A, Torpier G, Cecchelli R. A new function for the LDL receptor: transcytosis of LDL across the blood–brain barrier. *J Cell Biol*. 1997;138:877–889.
39. Elshourbagy NA, Liao WS, Mahley RW, Taylor JM. Apolipoprotein E mRNA is abundant in the brain and adrenals, as well as in the liver, and is present in other peripheral tissues of rats and marmosets. *Proc Natl Acad Sci U S A*. 1985;82:203–207.
40. Riad M, Tong XK, Mestikawy SE, Hamon M, Hamel E, Descarries L. Endothelial expression of the 5-hydoroxytriptamine$_{1B}$ anti-migraine drug receptor in rat and human brain vessels. *Neuroscience*. 1998;86:1031–1035.
41. Gobbi M, Re F, Canovi M, et al. Lipid-based nanoparticles with high binding affinity for amyloid-β_{1-42} peptide. *Biomaterials*. 2010;31:6519–6529.
42. Shaykhalishahi H, Taghizadeh M, Yazdanparast R, Chang YT. Anti-amyloidogenic effect of AA3E2 attenuates beta-amyloid induced toxicity in SK-N-MC cells. *Chem Biol Interact*. 2010;186:16–23.
43. Shibata A, Ikawa K, Shimooka T, Terada H. Significant stabilization of the phosphatidylcholine bilayer structure by incorporation of small amounts of cardiolipin. *Biochim Biophys Acta*. 1994;1192:71–78.
44. Bulbarelli A, Lonati E, Cazzaniga E, et al. TrkA pathway activation induced by amyloid-beta (Abeta). *Mol Cell Neurosci*. 2009;40:365–373.
45. Niewiadomska G, Mietelska-Porowska A, Mazurkiewicz M. The cholinergic system, nerve growth factor and the cytoskeleton. *Behav Brain Res*. 2011;221:515−526.
46. Bu G. Apolipoprotein E and its receptors in Alzheimer's disease: pathways, pathogenesis and therapy. *Nat Rev Neurosci*. 2009;10:333–344.
47. Hirst WD, Stean TO, Rogers DC, et al. SB-399885 is a potent, selective 5-HT6 receptor antagonist with cognitive enhancing properties in aged rat water maze and novel object recognition models. *Eur J Pharmacol*. 2006;553:109–119.
48. Kuo YC, Lin CY. Targeting delivery of liposomes with conjugated p-aminophenyl-α-D-manno-pyranoside and apolipoprotein E for inhibiting neuronal degeneration insulted with β-amyloid peptide. *J Drug Target*. 2015;23:147–158.
49. Negre-Salvayre A, Coatrieux C, Ingueneau C, Salvayre R. Advanced lipid peroxidation end products in oxidative damage to proteins. Potential role in diseases and therapeutic prospects for the inhibitors. *Brit J Pharmacol*. 2008;153:6–20.
50. Lovell M, Ehmann W, Butler S, Markesbery W. Elevated thiobarbituric acid-reactive substances and antioxidant enzyme activity in the brain in Alzheimer's disease. *Neurology*. 1995;45:1594–1601.
51. Pratico D, Uryu K, Leight S, Trojanoswki JQ, Lee VM. Increased lipid peroxidation precedes amyloid plaque formation in an animal model of Alzheimer amyloidosis. *Neuroscience*. 2001;21:4183–4187.
52. Garcia-Ayllon MS, Silveyra MX, Saez-Valero J. Association between acetylcholinesterase and beta-amyloid peptide in Alzheimer's cerebrospinal fluid. *Chem Biol Interact*. 2008;175:209–215.
53. Melo JB, Agostinho P, Oliveira CR. Involvement of oxidative stress in the enhancement of acetylcholinesterase activity induced by amyloid beta-peptide. *Neurosci Res*. 2003;45:117–127.
54. Bentue-Ferrer D, Reymann JM, Rousselle JC, et al. 5-HT-moduline, a 5-HT$_{1B/1D}$ receptor endogenous modulator, interacts with dopamine release measured in vivo by microdialysis. *Eur J Pharmacol*. 1998;358:129–137.
55. Mauch DH, Nagler K, Schumacher S, et al. CNS synaptogenesis promoted by glia-derived cholesterol. *Science*. 2001;294:1354–1357.
56. Charles V, Mufson EJ, Friden PM, Bartus RT, Kordower JH. Atrophy of cholinergic basal forebrain neurons following excitotoxic cortical lesions is reversed by intravenous administration of an NGF conjugate. *Brain Res*. 1996;728:193–203.